Spiral Spin Order of Self-Assembled Co Nanodisk Arrays

Youhui Gao,[1,3,*] Yuping Bao,[2] Alec B. Pakhomov,[2] Daisuke Shindo,[3] and Kannan M. Krishnan[2,†]

[1]*Department of Physics, Beijing Normal University, Beijing 100875, People's Republic of China*
[2]*Department of Materials Science and Engineering, University of Washington, Box 252120, Seattle, Washington 98195, USA*
[3]*Institute of Multidisciplinary Research for Advanced Materials, Tohoku University, 1-1 Katahira, 2-Chome, Aobaku, Sendai 980-8577, Japan*

(Received 5 January 2005; revised manuscript received 17 November 2005; published 7 April 2006)

Spin order in hexagonal close packed cobalt nanodisk rows is quantitatively determined by off-axis electron holography. Periodic variation in the density of the local magnetic flux shows features of a spiral spin arrangement along the row axis, resulting from a tilted magnetic moment of nanoparticles with respect to the nanodisk axis.

DOI: 10.1103/PhysRevLett.96.137205 PACS numbers: 75.75.+a, 42.40.Kw

Magnetic nanocrystals (MNCs) display novel electronic, magnetic, optical, and structural properties attributed to their small size and large fraction of surface atoms. Rapid and continuous progress in research in this field is expected to produce an entire generation of new devices of fundamental interest and potential technological applications in a variety of fields, ranging from biomedical research to information technology [1–5]. In addition to the tiny volume, the geometric order and specific functions of such devices can be reproduced, and their properties can be controlled at the nanometer scale by self-assembly of the nanocrystals. The self-assembling behaviors of MNCs are governed mainly by four energy contributions, given by:

$$E = \sum_{i,j}(E_r^{ij} + E_v^{ij} + E_d^{ij}) + \sum_i E_h^i. \quad (1)$$

E_r^{ij} is the energy of repulsive force among MNCs caused by the organic surfactant, which is a necessary requirement to prevent crystals from aggregation and retain long term stability for their colloidal dispersions. E_v^{ij} is the energy of van der Waals attraction. Both of them are functions of the number and the distance of the nearest neighbors; i.e., they are short-ranged. Balance between the repulsive force and the van der Waals attraction tends to produce two- and three-dimensional periodic self-organization [6–8]. E_d^{ij} is the energy of dipolar interaction, which is proportional to the magnetic moments of individual crystals. MNCs in the dispersion are coupled to each other by this long-ranged interaction. Motion of one crystal induced by a thermal disturb always influences that of its surroundings. A variety of self-assembly patterns as a function of crystal size can be produced [9–11]. E_h^i is the energy of MNCs in a magnetic field. It offers the means to artificially control the self-assemblies of MNCs [10].

An equilibrium assembly of MNCs corresponding to a minimum value of E indicates two structural orders: One is geometric order that describes the spatial organization of the crystals; the other one is magnetic order that pictures magnetic spin texture in the assembly induced by the dipolar interaction (and/or the external field if it is not zero). Recently, fabrication and superlattice of nanocrystals have been the focus of much attention. However, very little work has been done on characterizing the spin texture in MNC assemblies, which needs application of sophisticated techniques. The spin order is indispensable to understanding the effects of dipolar interactions on the self-assembling behavior of MNCs and also of vital importance for some technological applications, such as magnetic storage, spin-dependent tunnel nanojunction [12], and biomedical applications [13]. Here we suggest a spiral spin order in a cobalt nanodisk (ND) array based on *quantitative* measurements using off-axis electron holography. The magnetic properties of the ND rows are deduced from SQUID measurement on thick (3D) samples by extraction of a superparamagnetic contribution. We choose to study disk-shaped MNCs for the reason that they are particularly interesting from both fundamental and application perspectives and also because they exhibit a lesser degree of freedom for Brownian movement in the colloidal dispersion compared to spherical particles so that the observed results can be easily analyzed.

Cobalt NDs are fabricated by a modified La Mer method [9,11,14]. A surfactant mixture of oleic acid and linear amines is used to control the growth rates of different crystalline faces. The resulting crystals encapsulated in a 2-nm-thick surfactant layer are then dispersed in toluene subsequent to a size-selective precipitation procedure and deposited onto amorphous carbon-coated copper grids by a gradient evaporation process as reported in Ref. [11]. High-resolution transmission electron microscopy (TEM) indicates that the crystals are crystallized in the hexagonal close packed (hcp) structure with a sharp size distribution [about 18 nm in diameter and 5 nm in thickness as shown in Fig. 1(a)] but contain abundant stacking faults. The crystal direction of [002] is parallel to the electron trajectory. Each Co ND is a single-domain magnet. Neglecting the surface and shape anisotropy, its anisotropy energy KV, where K is the anisotropic constant of hcp-Co and V is the ND volume, is about $160k_BT$, where k_B is Boltzman's constant

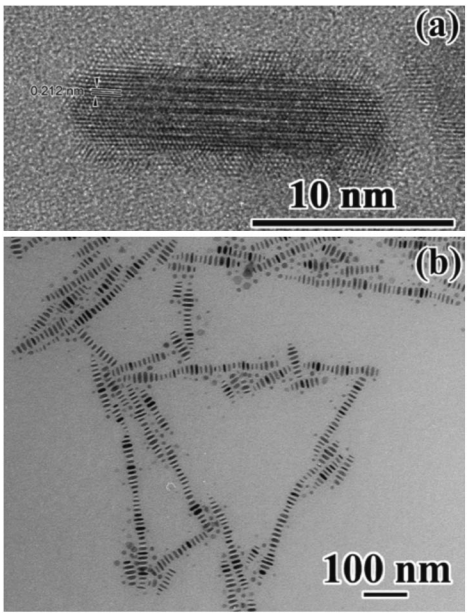

FIG. 1. (a) High-resolution TEM image. The nanodisks exhibit hexagonal close packed crystal structure with the magnetic easy axis [002] parallel to the electron trajectory. The crystal contains some stacking defects. (b) TEM bright-field image of cobalt nanodisk rows. The row unit consisting of ~7 nanodisks shows a spindle shape to decrease the magnetostatic energy. Several units construct a long nanodisk row.

and T is the room temperature 300 K. This energy barrier is big enough to pin the ND magnetic moment along its effective easy axis. The above dispersion condition produces self-assembled ND rows with an average interparticle distance of 4 nm [Fig. 1(b)]. The row axes are randomly oriented in plane. It is worth noting that a unit consisting of ~7 NDs shows a *spindle* shape, in which small disks appear at its two ends, and several units construct a long and flexible ND row. This arrangement may be due to depletion forces in the system with broad particle size distribution [11]. In order to minimize the magnetostatic energy, the ND rows can have a spin order of either ferromagnetic longitudinal (FL) configuration, where the spins are aligned head to tail along the row axis, or antiferromagnetic transverse (AFT) configuration, where the spins are perpendicular to the row axis and antiparallel to their nearest neighbors. However, our results indicate a possibility of an intermediate magnetic order where moments are arranged in a spiral configuration. This suggestion follows from a *direct* measurement by off-axis electron holography, a technique to visualize magnetic flux with nanometer spatial resolution [15–17], of the distribution of the local magnetic fields in the ND rows.

The electron holography is carried out at room temperature at an accelerating voltage of 200 kV with a JEM 3000F field-emission-gun TEM, which is equipped with a special pole piece to shield the sample from the field of the objective lens. A positive voltage of 40 V is applied to an electrostatic biprism wire in order to overlap the object electron wave with the reference wave. The phase shift arising from both the mean inner potential (ϕ_{MIP}) and from the magnetic induction (ϕ_{MAG}) of NDs is given by the following expression [15]:

$$\phi(x, y, z) = \frac{2\pi}{\lambda U(1 + \sqrt{1 - (\nu/c)^2})} \int V(x, y, z)dz + \frac{e}{\hbar} \iint B_n ds, \quad (2)$$

where B_n is the in-plane component of the magnetic induction, z is the incident electron beam direction, U is the TEM accelerating voltage, λ is the wavelength, and ν and c are electron and light velocities, respectively. For the NDs of interest here, ϕ_{MIP} [the first term in Eq. (2)], calculated on the assumptions that $V(x, y, z) = 26$ V [18] and $B_n = 1.7$ T, is about 1.1π rads, much bigger than that of ϕ_{MAG} (0.2π rads). In order to quantify the contribution of magnetic induction, in the present study ϕ_{MIP} is removed from the reconstructed phase image using the method proposed in Ref. [16].

A typical bright-field TEM image of cobalt ND rows and a corresponding reconstructed phase image, obtained from the magnetic contribution to the phase shift when it is examined at the remanent state, are shown in Figs. 2(a) and 2(b), respectively. The density of the contours in Fig. 2(b), which is proportional to the in-plane component of the magnetic induction B_n integrated in the electron beam direction, provides a quantitative measure of the strength and the direction of the local magnetic flux density. It is found that the row unit exhibits a contour profile similar to a solenoid. Continuous contours run through all NDs in the direction of the row axis, suggesting that the AFT spin order does not exist in the ND rows at all. On the other hand, it is also found that the direction and the density of the contours in the ND rows slightly fluctuate along the axis (angle variation within roughly $\pm 10°$–$20°$), reflecting that both the direction and the strength of the in-plane component of magnetic induction B_n are functions of the ND position. Thus, a pure FL situation may be not realized either.

Contour spacing (l) in the reconstructed phase image represents a magnetic flux of 4.1×10^{-15} Wb if the amplification of the phase shift is one [15,17]. The local B_n is inversely proportional to l and approximately determined from the equation

$$B_n = \frac{2\pi}{Alt_z} \cdot \frac{\hbar}{e} = \frac{4.1 \times 10^{-15}}{Alt_z} \ (\mathrm{Wb/m^2}), \quad (3)$$

where t_z is the sample thickness, and A is the phase shift amplification. Figure 2(c) shows the distribution of B_n along the row axis estimated by counting the local l of the contours. The result is somewhat appealing, as the in-plane component of magnetic induction shows periodic variation. The periodicity is about 45 nm, consisting of

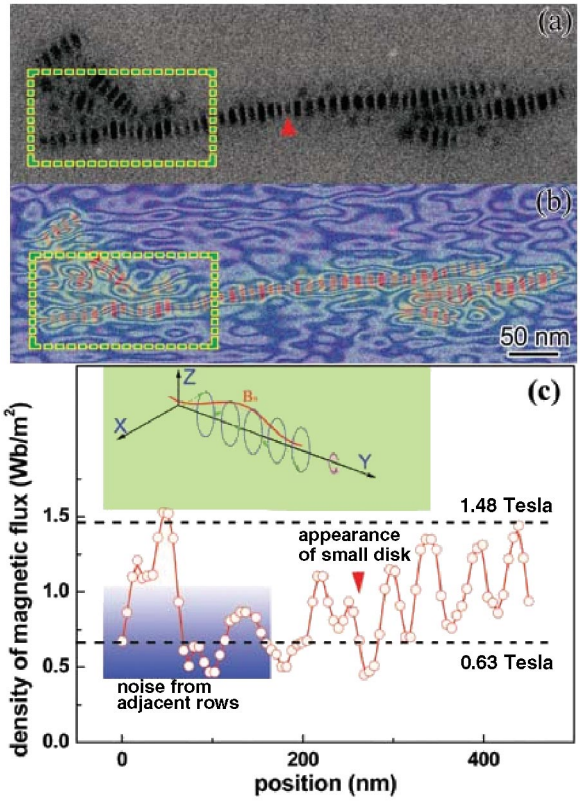

FIG. 2 (color). (a) TEM bright-field image of nanodisk rows. (b) The corresponding holographic image superimposed on the rainbow-type image of (a). Contours with a minimum width of 3.8 nm and a maximum width of 9.0 nm are formed, corresponding to in-plane magnetic induction components of 1.48 and 0.63 T, respectively. (c) Periodic variation of the in-plane component of magnetic induction estimated from the contour space. The inset shows the spiral spin order in the disk row. The periodicity of the spiral spin arrangement is about 45 nm, consisting of 4–5 nanodisks. The neighboring rows produce some noise as shown by blue shadows. The appearance of small disks [arrows in (a) and (b)] greatly affects the periodicity and magnitude of in-plane component magnetic induction.

4–5 NDs. A maximum $B_n = 1.48$ T is observed, smaller than the saturation magnetic induction of bulk hcp-Co (1.7 T). It may result from an overestimation of the sample thickness in the calculation. A minimum B_n of 0.63 T is also evaluated at regions of wide contours. The analysis of the electron holography indicates that the ND moment is tilted with respect to the projected plane of the electron beam, and the angle periodically changes with the position of the crystals. The proposed spin arrangement is sketched in the inset in Fig. 2(c), which is spiral-like and turning around the row axis. Apparently, this order is associated with the tilt of magnetic moments of individual hcp NDs due to the interplay of magnetic anisotropies. The energy balance leading to this magnetic arrangement needs a separate investigation. From the ratio of the minimum to maximum value of B_n, the angle between spin and row axis is estimated at about 68°; i.e., the effective easy axis of each ND deviates from the crystal direction of [002] about 22°. Note that the irregular long-range fluctuations of B_n in the region shadowed in Fig. 2(c) result from the noise produced by the neighboring rows [see the marked region in Fig. 2(a)]. Statistically, the period of variation of the magnitude of B_n correlates with the period of gray scale intensity, or particle sizes, based on the analysis of Fig. 2(a) (not shown here), or the appearance of small disks, as shown by red arrows in Figs. 2(a) and 2(c).

The ferromagnetic component of magnetization at room temperature associated with the spindle-shaped NP rows in the samples can be confirmed and studied by magnetic measurements. For these measurements, a *thick* film consisting of 7-ND units randomly dispersed in a matrix was deposited by ND colloidal dispersion diluted by a large volume of smaller cobalt particles not organized into rows (about 90% in the present study as follows from the analysis). The latter are superparamagnetic at room temperature. Assuming that the magnetic interaction between the ND rows and the small particles in the matrix is negligible, the SQUID result obtained at room temperature can be separated into a superparamagnetic and a ferromagnetic contribution. In order to remove the superparamagnetic signal, we first determine the mean size and the size distribution of the small particles as follows. The sample is cooled in a zero magnetic field from room temperature to 5 K. A field of 2 Oe is then applied, and the initial susceptibility χ_i is measured with increasing temperature. The zero field cooled-field cooled (ZFC-FC) magnetization curves show an apparent blocking temperature of small nanoparticles T_{B1} (defined as a maximum of the ZFC curve) below room temperature, while the ZFC magnetization continues to increase above 300 K ($T_{B2} > 300$ K associated with rows of NDs). A plot of the temperature derivative $d\Delta\chi_i/dT$, where $\Delta\chi_i$ is the difference between ZFC and FC susceptibilities, against temperature T is proportional to the distribution of blocking temperatures [19] and is shown in Fig. 3. The curve exhibits a broad peak at a temperature

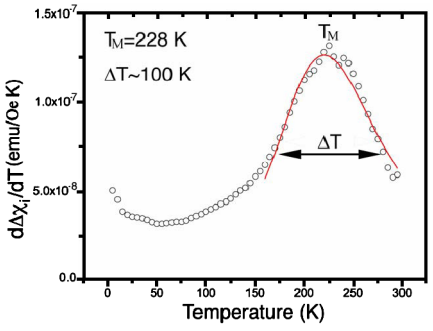

FIG. 3 (color online). Plot of $d\Delta\chi_\iota/dT$ vs T is fitted by a log-normal distribution function (solid curve), and the mean size and the size distribution width are estimated at 149 and 65 nm^3, respectively.

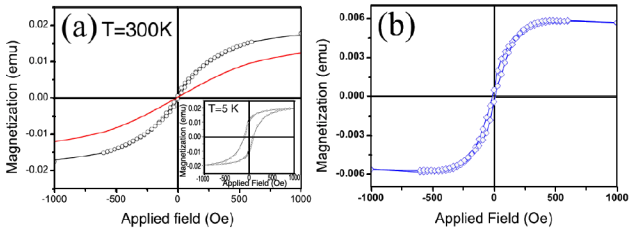

FIG. 4 (color online). Loops of thick film measured by SQUID at (a) 300 and (inset) 5 K. The solid curve in (a) is the superparamagnetic signal of the small particles calculated by the Langevin function. (b) is the loop of ND rows at $T = 300$ K obtained by subtracting the superparamagentic signal from the SQUID result.

T_M, defined as the average blocking temperature of the small particles, and the peak width ΔT is associated with the width of the particle volume distribution. Fitted by a log-normal function (the solid curve in Fig. 3), T_M and ΔT are evaluated as 228 and 100 K, respectively, corresponding to the mean volume of $\langle V \rangle = 149$ nm^3, or the mean diameter $\langle D \rangle \approx 6.6$ nm assuming a spherical shape of small nanoparticles, and the width of volume distribution of $\Delta V = 65$ nm^3 calculated using the blocking criteria $KV \sim 25 k_B T_B$ for individual MNCs and an assumption that K of hcp-Co is independent of T in the measurement temperature range.

Hysteresis loops for the thick film observed at 300 and 5 K are shown in Fig. 4(a) and the inset. It is found that the loop at 5 K has a shape typical of nanocrystalline magnetic materials (inset) where all Co crystals are blocked and has a coercivity H_c of 900 Oe and a reduced remanence M_r/M_s of 0.45. At 300 K, however, the major contribution in the loop is from superparamagnetic particles. Very small H_c and M_r/M_s are obtained. According to the concentration and the size distribution of the small particles, the superparamagnetic signal is approximated by the Langevin function [the solid curve in Fig. 4(a)], which is then subtracted from the total signal. The remaining moment associated with nanodisk rows $M_{\mathrm{ND}}(H)$ is plotted in Fig. 4(b). The loop is characterized by $H_c \sim 16$ Oe and $M_r/M_s \sim 0.1$. The abnormally low remanence is then attributed partially to the spiral spin arrangement (analogous to magnetic vortex in bulk magnetic materials) and partially to the temperature effects.

In conclusion, a spiral spin order in cobalt nanodisk rows, which results from a collective Brownian rotation during solvent evaporation, has been characterized by off-axis electron holography. This feature offers a unique opportunity to study magnetism on the nanoscale and shows that the magnetization behavior and reversal typical of the buckling mode can be pictured with these discrete single-domain nanocrystals.

Y. G. is supported by the 21st century COE program of Materials Research Center, Tohoku University. Work at the University of Washington was supported by NSF/DMR under Grants No. 0203069 and No. 0501421 and by the Campbell Endowment. Y. B. acknowledges partial support from UW/PNNL Joint Institute of Nanoscience.

*Permanent address: Department of Physics, Beijing Normal University, Beijing 100875, People's Republic of China.
To whom all correspondence should be addressed.
Electronic address: ygao@bnu.edu.cn
†Electronic address: kannanmk@u.washington.edu

[1] C. M. Leiber, Solid State Commun. **107**, 607 (1998).
[2] D. J. Wales, Science **271**, 925 (1996); all the review articles in the February 16, 1996 issue of Science.
[3] J. M. Perez, L. Josephson, T. O'Loughlin, D. Hogemann, and R. Weissleder, Nat. Biotechnol. **20**, 816 (2002).
[4] H. Gu, P. L. Ho, K. W. Tsang, L. Wang, and B. Xu, J. Am. Chem. Soc. **125**, 15 702 (2003).
[5] C. J. Meyer, F. J. Alenghat, P. Rim, J. H. Fong, B. Fabry, and D. E. Ingber, Nat. Cell Biol. **2**, 666 (2000); M. E. Chicurel, R. H. Singer, C. J. Meyer, and D. E. Ingber, Nature (London) **392**, 739 (1998); J. Chen, B. Fabry, E. L. Schiffrin, and N. Wang, Am. J. Physiol. **263**, C700 (1992).
[6] R. P. Andres, J. D. Bielefeld, J. I. Henderson, D. B. Janes, V. R. Kolagunta, C. P. Kubiak, W. J. Mahoney, and R. G. Osifchin, Science **273**, 1690 (1996).
[7] Z. L. Wang, Adv. Mater. **10**, 13 (1998).
[8] C. B. Murry, S. Sun, W. Gaschler, H. Doyle, T. A. Betley, and C. R. Kagan, IBM J. Res. Dev. **45**, 47 (2001).
[9] V. F. Puntes, K. M. Krishnan, and A. P. Alivisatos, Science **291**, 2115 (2001).
[10] Y. Gao, Y. Bao, M. Beerman, A. Yasuhara, D. Shindo, and K. M. Krishnan, Appl. Phys. Lett. **84**, 3361 (2004).
[11] Y. Bao, M. Beerman, and K. M. Krishnan, J. Magn. Magn. Mater. **266**, L245 (2003).
[12] C. T. Black, C. B. Murry, R. L. Sandstorm, and S. Sun, Science **290**, 1131 (2000).
[13] P. Gould, Mater. Today **7**, No. 2, 36 (2004).
[14] V. K. La Mer and R. H. Dinegar, J. Am. Chem. Soc. **72**, 4847 (1950).
[15] D. Shindo and T. Oikawa, *Analytical Electron Microscopy for Materials Science* (Springer-Verlag, Tokyo, 2002).
[16] R. E. Dunin-Borkowski, M. R. McCartney, D. J. Smith, and S. S. P. Parkin, Ultramicroscopy **74**, 61 (1998).
[17] R. E. Dunin-Borkowski, M. R. McCartney, R. B. Frankel, D. A. Bazylinski, M. Posfai, and P. R. Buseck, Science **282**, 1868 (1998).
[18] M. de Graef, T. Nuhfer, and M. R. McCartney, J. Microsc. **194**, 84 (1999).
[19] J. C. Denardin, A. L. Brandl, M. Knobel, P. Panissod, A. B. Pakhomov, H. Liu, and X. X. Zhang, Phys. Rev. B **65**, 064422 (2002).